ChemPubSoc Europe

DOI: 10.1002/cphc.201200759

The Electrochemical Properties of Nanocomposite Films Obtained by Chemical In Situ Polymerization of Aniline and Carbon Nanostructures

Marta E. Plonska-Brzezinska,*[a] Joanna Breczko,[a] Barbara Palys,[c] and Luis Echegoyen*[b]

Interactions between the π bonds in the aromatic rings of polyaniline (PANI) with carbon nanostructures (CNs) facilitate charge transfer between the two components. Different types of phenyleneamine-terminated CNs, including carbon nano-onions (CNOs) and single-walled and multi-walled carbon nanotubes (SWNTs and MWNTs, respectively), were prepared as templates, and the CN/PANI nanocomposites were easily prepared with uniform core–shell structures. By varying the ratio of the aniline monomers relative to the CNs in the in situ chemical polymerization process, the thickness of the PANI layers was effectively controlled. The morphological and electrical properties of the nanocomposite were determined and compared. The thickness and structure of the PANI films on the CNs were characterized by transmission electron microscopy (TEM), scanning electron microscopy (SEM), and infrared spectroscopy. TEM and SEM revealed that the composite films consisted of nanoporous networks of CNs coated with polymeric aniline. The electrochemical properties of the composites were investigated by cyclic voltammetry and electrochemical impedance spectroscopy. These studies showed that the CN/PANI composite films had lower resistance than pure polymeric films of PANI, and the presence of CNs much improved the mechanical stability. The specific electrochemical capacitance of the CNO/PANI composite films was significantly larger than for pure PANI.

1. Introduction

Electrochemical supercapacitors are very attractive power sources because of their high specific power and very long durability.[1] In electrochemical capacitors, the charge is accumulated in the electrical double layer at the electrode/electrolyte interface. The main advantage of an electrochemical double-layer capacitor (EDLC) is its ability to discharge very quickly. Materials usually employed to prepare supercapacitors include carbon,[2,3] metal oxides,[4–6] and electrically conducting polymers (ECPs), such as polyaniline (PANI),[7] polypyrrole,[8] and polythiophene.[9] ECPs have larger pseudocapacitances than carbon materials. Electrochemical supercapacitors that have a carbon electrode component can be classified into two types depending on the charge-storage mechanism that is present. In the first case, a pure electrostatic attraction exists between the charged surface of the electrode and the ions in the EDLCs. In the second type, the pseudocapacitors, electrons are involved in charging the double layer and in quick faradaic reactions.[10] The capacitance values depend on the nature of the electrode/electrolyte interface and/or the amount of pseudocapacitive additives.[11,12]

PANI is one of the most studied conducting polymers partly because the monomer is inexpensive and easily available and also because of its unique proton doping mechanism.[13] The reported specific capacitance of pure PANI is very high (720 $F g^{-1}$),[14] but its application in supercapacitor electrodes is limited, partly because of poor electrochemical stability during the cycling. PANI exhibits slow ion-transport kinetics, because the redox sites in the polymer backbone are not sufficiently stable during the multiple cycles.[15] Suitable materials with high stability, conductivity, nanosize, and high surface area have been considered as fillers to overcome the stability problem and to enable fast transport of counterions across and within the polymer films.

Carbon nanostructures (CNs) hold great promise as reinforcing phases in novel composite materials. In particular, composites of carbon nanotubes (CNTs) and polymers have been extensively studied.[16–18] These composites have a polymeric-nanostructured matrix that exhibits cooperative behavior between the host and guest and modifies the electronic properties of both components. Such materials have great potential in electrotechnology and, in particular, in the production of porous electrodes as electrochemical supercapacitors. Composites of CNTs and electrochemically active π-conjugated con-

[a] Dr. M. E. Plonska-Brzezinska, J. Breczko
Institute of Chemistry
University of Bialystok
Hurtowa 1
15-399 Bialystok (Poland)
E-mail: mplonska@uwb.edu.pl

[b] Prof. Dr. L. Echegoyen
Department of Chemistry
University of Texas at El Paso
500 W. University Ave.
El Paso, TX 79968 (USA)
E-mail: echegoyen@utep.edu

[c] Dr. B. Palys
Faculty of Chemistry
University of Warsaw
Pasteura 1
02-093 Warsaw (Poland)

ducting polymers, such as polypyrrole,[19] PANI,[13–15,20] and polythiophene,[21] are usually used as redox capacitors. In those cases, polymer oxidation results in charge accumulation in the composite. The presence of CNs in these composites significantly enhances the capacitive properties of the polymeric host.

High surface area is important for hybrid composites in which CNs are used as a template. These properties are essential for obtaining high specific capacitances. The capacitance of CN/PANI nanocomposites depends on the diameter and length of the carbon structures, their distribution in the polymer network, the ratio of CNs to conducting polymer, and the concentrations and types of impurities.[22] Therefore, the supercapacitive characteristics of CN/PANI composites depend on the deposition of the PANI and its morphology,[23–25] the electrolyte used in the synthesis,[26,27] and the various aniline derivatives utilized.[28,29] Recent studies have shown that the introduction of CNs to PANI can enhance the electrical properties by facilitating charge-transfer processes between the two components.[30] Many efforts have been focused on the design and preparation of CN/PANI composites. For instance, a specific capacitance of 463 $F g^{-1}$ was achieved for single-walled nanotubes (SWNTs) deposited by electrochemical polymerization with 73 wt.% PANI,[31] and a specific capacitance of 500 $F g^{-1}$ was achieved for multi-walled carbon nanotube (MWNT)/PANI composites containing 0.8 wt.% MWNTs.[32] The electrochemical and pseudocapacitive properties of MWNT/PANI composites were investigated by doping and dedoping for different compositions of the emeraldine salt form.[33] The MWNT/PANI nanocomposites showed specific capacitance values of 217, 328, and 139 $F g^{-1}$ for leucoemeraldine base, emeraldine salt, and pernigraniline base, respectively. PANI/coated buckypaper composite electrodes, prepared from MWNTs (424 $F g^{-1}$), possess a specific capacitance that is almost five times higher than that of MWNT/PANI prepared under the same conditions.[34] Li et al. prepared ordered mesoporous carbon/PANI through in situ polymerization, and the composite exhibited a specific capacitance of 747 $F g^{-1}$.[35] The highest specific capacitance of 1046 $F g^{-1}$ and excellent cycle stability was obtained for a graphene nanosheet/PANI composite in 6 M KOH.[36]

Our recent research work has been centered mainly on carbon-based materials, such as carbon nano-onions (CNOs). A fullerene-like CNO structure was first observed by Ugarte in 1992,[37] although similar structures were previously seen by Iijima in 1980.[38,39] The CNO structures consist of a hollow spherical fullerene core surrounded by concentric and bigger fullerenes with increasing diameters. The distance between the fullerene layers is very close to the interlayer distance in bulk graphite (0.34 nm).[40] CNO structures (5–6 nm in diameter, 6–8 shells) can be obtained by high-temperature annealing of ultradispersed nanodiamonds (5 nm, average diameter), which leads to their transformation into CNO structures (5–6 nm in diameter, 6–8 shells).[41] CNOs have a variety of potential applications, including optical limiting,[42] field emission in solar cells,[43] fuel cell electrodes,[44] hyperlubricants,[45] biosensor,[46] and materials and composite electrodes.[47,48]

Both types of CNs, CNOs and CNTs, have high conductivity and large surface area. Because of the unique structural, mechanical, and electronic properties of CNs, they are potentially excellent fillers to improve the electrical conductivity and mechanical properties of polymers. To date, this potential has not yet been fully realized, partly because it is difficult to obtain uniform dispersions of CNs within the polymer matrices.[1] CNs tend to aggregate, because of strong van der Waals interactions between them. Another challenge is to form strong physical and chemical bonds between the CNs and the polymer matrices.

The work reported here focuses on electrochemical studies of composites containing CNs, such as CNOs, SWNTs or MWNTs, and PANI. The main advantage of "small" CNOs (5–6 nm in diameter) over CNTs or "bigger" CNOs (20–100 nm in diameter) is their easier dispersion in aqueous solutions during the polymerization phase, which improves the homogeneity of the composites. To use these composites in supercapacitors and to obtain compositions with optimum specific capacitance values, it is important to correlate their microstructure with specific capacitances. The electrochemical and capacitance results presented in this article compare composites that were prepared under identical and controlled conditions so that CNO/PANI, MWNT/PANI, and SWNT/PANI form a homologous series. We refrain from comparing our results with those of other reports of CNT/PANI composites, because the synthetic methods are not identical and lead to materials with different properties.

2. Results and Discussion

The procedure for the functionalization of CNs with phenyleneamine-terminated groups was previously described.[49] To introduce functional groups onto the surfaces of CNs, 4-aminobenzoic acid (4-ABAc) was treated with the CNs. Next, in situ polymerization of aniline was performed on the surface carboxylic groups by using a procedure already described[49] to obtain the CN/PANI products (CN: CNO, SWNT, or MWNT).

To confirm the presence of PANI in the layer of the composite and its conducting character, the CN/PANI composites were studied by infrared (IR) spectroscopy (Figure 1). A large broad absorption peak observed between 3700 and 2500 cm^{-1} is frequently encountered in electrically conductive polymers as a result of electronic transitions from the valence band to the conducting band.[50] Earlier IR studies suggested that the absorption modes at about 1500 and 1600 cm^{-1} are associated with aromatic ring stretching vibrations. The spectra clearly exhibit the presence of benzenoid (B) and quinoid ring (Q) vibrations at 1500 and 1600 cm^{-1}, respectively.[51,52] The intensities indicate an enhanced benzenoid/quinoid ratio and confirmed the oxidation state of PANI. The intensity of the quinoid band increases as the oxidation degree of the polymer increases.[53] Therefore, the high intensity of the 1311–1313 cm^{-1} peaks suggest that PANI is in its semioxidized conductive form. The very weak and broad band near 3400 cm^{-1} is assigned to the N–H stretching mode of the NH and NH_2 groups. The difference between the spectra in Figure 1 is clear in the N–H stretching

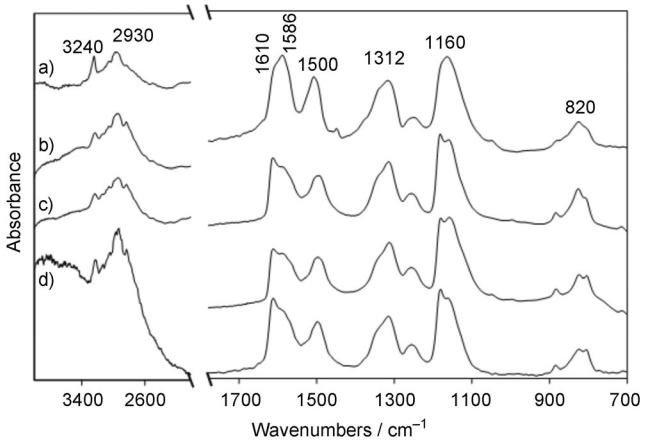

Figure 1. FTIR microscope spectra in the range 4000–700 cm^{-1} of a) CNO/PANI, b) SWNT/PANI, c) MWNT/PANI, and d) PANI.

region. This signal is broad and strong for the composite samples, whereas a very weak spectrum is observed for pure PANI. The interaction between PANI and the CNs most likely involves "charge transfer", as suggested previously.[51,52] The vibrational modes in the range of 1155–1160 cm^{-1} are associated with C–H bending modes of the benzenoid and quinoid rings.[54,55] These modes were described as an "electronic-like band" and are considered to be a measure of the degree of delocalization of the electrons, and thus this characteristic band is indicative of PANI conductivity.[51,52] Analysis of the Fourier transform (FT)IR spectra of the CN/PANI composites indicates that PANI was effectively deposited on the surface of the CNs to form nanocomposites and that the polymer exhibits conductive behavior.

Figure 2 shows the typical high-resolution transmission electron microscopy (HRTEM) images for the CN/PANI composites. The TEM images clearly illustrate that the CNs are covered by a compact PANI layer. It has been demonstrated that such CNs can act as good templates for the formation of uniform core–shell-structured CN/PANI composites. From TEM observations, it was found that the diameters of the modified CNs were about 8–15, 40, and 50 nm for CNOs, SWNTs, and MWNTs, respectively.

The desired characteristics of carbon materials for electrochemical applications include wettability and high conductivity. Wettability is generally improved by the presence of surface functionalities, whereas electrical conductivity depends mainly on the nanotexture.[1] The nanotextural properties of carbon are characterized by its specific surface area, the presence of micro- and mesopores, and their shapes. High surface area is required for high-performance supercapacitors.

Scanning electron microscopy (SEM) images of a Au foil covered with CN/4-ABAc and CN/PANI composites are shown in Figure 3. The structures exhibit porous morphologies, with many channels and outcroppings. The modification of the structures of the CNs by oxidation with 4-ABAc did not change the initial nanostructure of the carbon materials, that is, CNTs or CNOs (Figure 3a, d, g), and gave rise to increased solubilities and ease of surface film formation. The morphology of the CNs

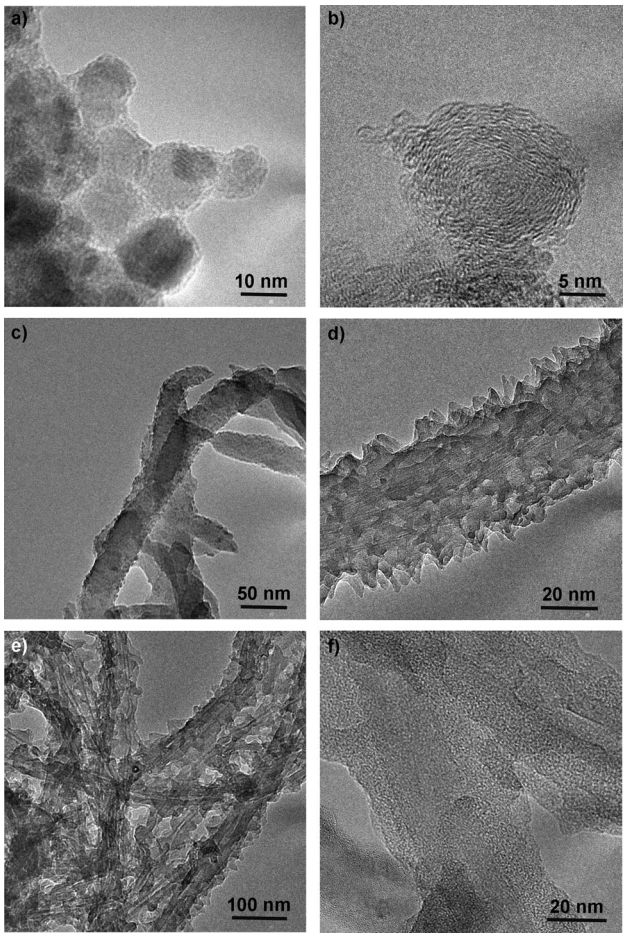

Figure 2. HRTEM images of a), b) CNO/PANI, c), d) SWNT/PANI, and e) f) MWNT/PANI ($m_{CNs}/m_{PANI} = 1:2$).

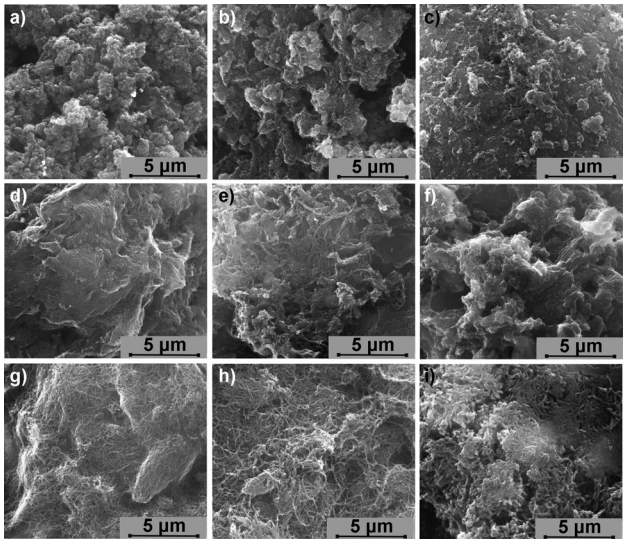

Figure 3. SEM images of the Au foil covered with a) CNO/4-ABAc, b) CNO/PANI ($m_{CNOs}/m_{PANI} = 2:1$), c) CNO/PANI ($m_{CNOs}/m_{PANI} = 1:2$), d) SWNTs/4-ABAc, e) SWNT/PANI ($m_{SWNTs}/m_{PANI} = 2:1$), f) SWNT/PANI ($m_{SWNTs}/m_{PANI} = 1:2$), g) MWNTs/4-ABAc, h) MWNT/PANI ($m_{MWNTs}/m_{PANI} = 2:1$), and i) MWNT/PANI ($m_{MWNTs}/m_{PANI} = 1:2$).

modified by 4-ABAc differs from that of films formed by the CN/PANI composites. The micrographs (Figure 3b, e, h) clearly reveal the wrapping by PANI and show a significant increase in the diameter of the CNs after composite formation. An additional increase in the concentration of the aniline monomer during the polymerization reaction resulted in an increase in the corresponding diameters of the carbon nanoparticles wrapped by the polymer (Figure 3c, f, i). These microstructural variations have a profound influence on the resulting capacitive behavior of the CN/PANI composites.

To elucidate the effect of the CN morphology on the electrochemical properties of the CN/PANI composites and the presence of PANI in the film, cyclic voltammetry (CV) studies were performed. The solid films of CN/PANI (CN: CNO, SWNT, or MWNT) were prepared by drop coating. The CN composites were sonicated in 0.1 M HCl solution. A drop of solution containing the dispersed functionalized CNs (CN/PANI) was then deposited on the electrode surface. After solvent evaporation, the electrode covered with the thin film of the modified CNs was transferred to an aqueous solution containing 0.1 M H_2SO_4 as the supporting electrolyte.

The CV responses of CN/PANI (CN: CNO, SWNT, or MWNT), and that of PANI for comparison, in monomer-free solution are shown in Figure 4. Our previous studies showed that the CNO/PANI films exhibit excellent mechanical and electrochemical stability under CV conditions within the potential range from −0.20 to +1.00 V versus Ag/AgCl.[51]

The characteristic CV response of PANI (Figure 4d) consists of three redox couples (Ox_1/R_1, Ox_2/R_2, and Ox_3/R_3), and these correspond to two-electron processes.[56,57] The Ox_1/R_1 peaks are attributed to the conversion of amine units to radical cations (semiquinones). The Ox_3/R_3 peaks are assigned to the redox reactions of the degradation products and to the conversion of the radical cation into the fully oxidized form of the polyaniline(quinonediimine). The peaks at +0.45 V versus Ag/AgCl (Ox_2/R_2) were identified as the ones belonging to water-soluble degradation products. At both positive and negative extremes of the potential scan, pure PANI and the CN nanocomposites turn into nonconducting forms. The voltammograms reveal that the CN/PANI films are stable in sulfuric acid solution within the scanned potential range. The CV traces for CN/PANI (Figure 4a–c) and for pure PANI (Figure 4d) show faradic responses arising from the contribution of the conducting polymer in the composites.

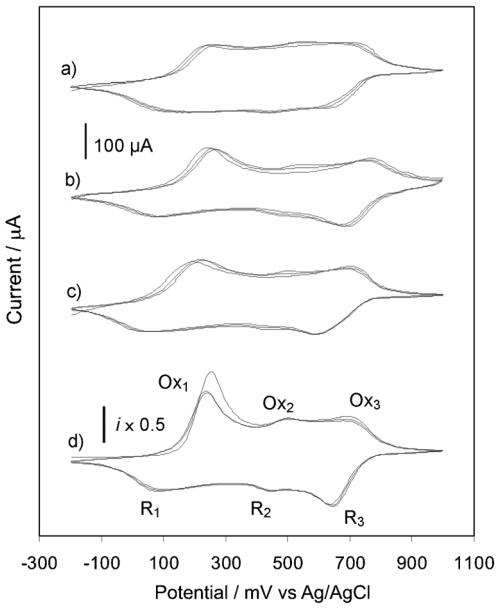

Figure 4. Cyclic voltammograms of the GC electrode covered with CN/PANI films (2:1 mass ratio CN/PANI): a) CNO b) SWNT, c) MWNT, and d) pure PANI for comparison (in 0.1 M H_2SO_4). The sweep rate was 20 mV s^{-1}.

The capacitive characteristics for the CN/PANI composites were examined by CV. Figure 5 shows a comparison of the electrochemical properties of the CN/PANI films containing the CNO-, SWNT-, and MWNT-modified nanostructures. The relative compositions of the CN/PANI samples were 9:1, 2:1, 1:2, and 1:9 mass ratio CNO/PANI and 2:1 and 1:2 mass ratio (SWNTs or MWNTs)/PANI. All films exhibit typical capacitive behavior. The voltammograms, with the potential cycled between +0.30 and +0.60 V versus Ag/AgCl, show almost pseudorectangular cathodic and anodic profiles, which is the characteristic behavior of an ideal capacitor.

As previously observed,[1] the capacitance current depends on film composition. Previous studies show that the specific capacitance (C_s) of the electrode can be estimated from the CV curves and by using Equation (1):

$$C_S = \frac{\int_{E_1}^{E_2} i(E)dE}{2vm(E_2 - E_1)} \quad (1)$$

in which C_s is the specific capacitance, E_1 and E_2 are the cutoff potentials in CV, $i(E)$ is the instantaneous current, $\int_{E_1}^{E_2} i(E)dE$ is the total voltammetric charge obtained by integration of the positive and negative sweeps in the cyclic voltammograms, and m is the mass of the individual sample. The values of C_s calculated from Equation (1) are collected in Table 1. For comparison, the specific capacitances of ox-CNO/tetraoctyloammonium bromide (TOABr)[47] and PANI films are also shown.

Figure 6 shows the voltammetric behavior of the CNO/PANI films in a 0.1 M H_2SO_4 aqueous solution at different sweep rates. The capacitive current varies linearly with the sweep rate at +0.50 V versus Ag/AgCl (Figure 6b). A linear dependence of the capacitive current with the sweep rate is observed over a large sweep rate range (up to 500 mV s^{-1}), as shown in Figure 6b. The capacitive current (i_c) is given by Equation (2):

$$i_c = C_s vm \quad (2)$$

in which C_s is the specific capacitance, m is the mass of the material deposited on the electrode surface, and v is the potential sweep rate. The values of the specific capacitances calculated from the dependence of the current with the scan rate for the different types of CNs modified by PANI are collected in Table 1. The values of the specific capacitances obtained by integration of I versus E curves are slightly different than those calculated from the linear relationship of the I versus v plots

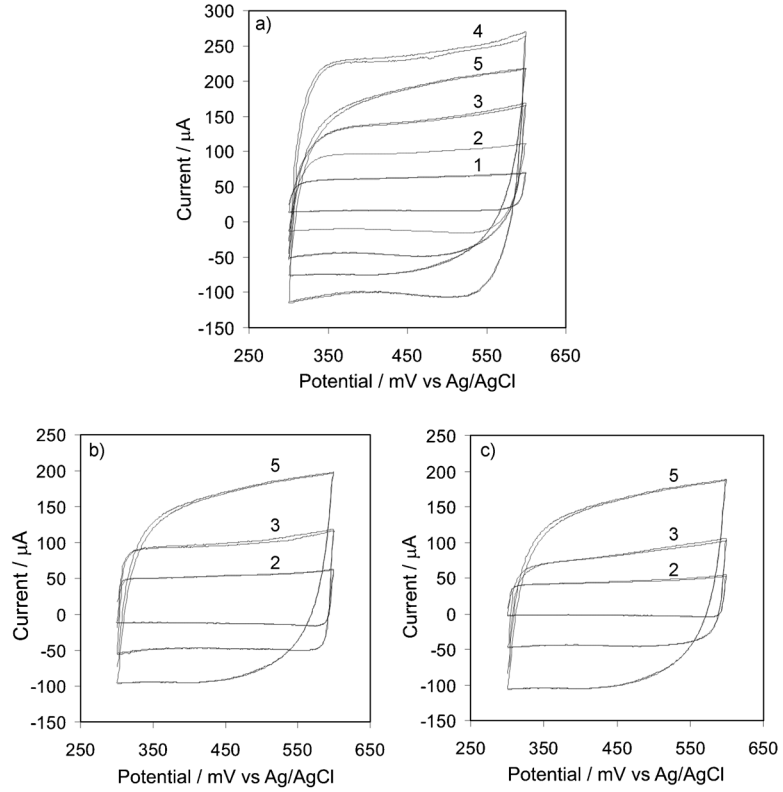

Figure 5. Cyclic voltammograms of the GC electrode covered with CN/PANI: a) CNO, b) SWNT, and c) MWNT. Mass ratio CN/PANI was 1) 9:1, 2) 2:1, 3) 1:2, 4) 1:9, and 5) pure PANI (in 0.1 M H_2SO_4). The sweep rate was 10 mV s^{-1}.

Table 1. Specific capacitance of CN/PANI composites obtained on the basis of voltammetric studies.

Composite	C_S [F g^{-1}][b]	
	Integration of i_c versus E voltammogram	Slope of i_c versus V relation
CNO/PANI[a]		
9:1	110	120
2:1	207	214
1:2	286	306
9:1	496	506
MWNT/PANI[a]		
2:1	153	170
1:2	268	280
SWNT/PANI[a]		
2:1	106	129
1:2	232	247
PANI	409	422
ox-CNO/TOABr[c,d]	2.90	2.29

[a] The m_{CNs}/m_{PANI} mass ratio in the composite. [b] Capacitance per gram of the composite. [c] Calculated capacitance of oxidized CNOs in 0.1 M NaCl from ref. [47]. [d] TOABr = tetraoctyloammonium bromide.

(Table 1). In both cases, specific capacitances of the CN/PANI films are affected by the nature of the CNs and the thickness of the PANI layer deposited on the CNs.

The highest observed specific capacitance of 506 F g^{-1} (see Table 1) was achieved with CNO nanostructures modified with a PANI layer (m_{CNOs}/m_{PANI} = 1:9). The high specific capacitance for the CNO/PANI composite, which is higher than that of pure PANI (422 F g^{-1}, see Table 1), is probably indicative of a selective interaction between the quinoid ring of the polymer and the CNO surface, and this provides a channel for charge transfer and storage. The favorable electronic properties and very good dispersion ability of the CNO/ABAc derivatives in the aniline monomer help to form better contacts between the CNO and PANI and, thus, to obtain a charge-transfer complex, which may provide higher conductivity. The larger surface area allows better electrolyte access, and this facilitates the charge-transfer process and reduces the internal resistance of the electrode. All of these result in more favorable electrochemical properties of the CNO/PANI (1:9) composites than for pure CNO and PANI films.

Electrochemical impedance spectroscopy (EIS) has been widely used to study the redox processes of ECPs and/or carbon materials. Figure 7 shows the EIS results obtained for the CNO/PANI films containing different amounts of CNOs with a conventional three-electrode electrochemical cell and an ac voltage amplitude of 5 mV over a frequency range of 10^{-1}–10^5 Hz in 0.1 M H_2SO_4 electrolyte. The complex impedance can be presented as the sum of the real (Z') and imaginary (Z'') components that originate mainly from the resistance and capacitance of the cell, respectively. Analysis of Figure 7a reveals that the EIS plot, which was obtained at E = 0 V versus Ag/AgCl, has two well-separated features. First, the high-frequency intercept of the semicircle resulting from an electron-transfer-limited process, which includes the resistance of the electrolyte solution, the intrinsic resistance of the active material, and the contact resistance at the active interface material/current collector. Second, a linear response at the low frequency end resulting from diffusion-controlled doping and undoping of the anions that lead to Warburg behavior (Z_W).[60]

The results of the impedance studies at the CNO/PANI films depend noticeably on the composition of the composite (Figure 7a) as well as on the electrode potential (Figure 7b). In spite of the similarities of the impedance spectra, there is an obvious difference between the diameters of the four semicircles (Figure 7a). The diameters of the semicircles decrease pronouncedly as the doping content of the CNOs in the composites is increased (Figure 7a) and as the applied potential is increased (Figure 7b). That is, the film transport of electrons and the charge-transfer resistance (R_{ct}) of the CNO/PANI composites are much lower than those of the pure PANI films. This means

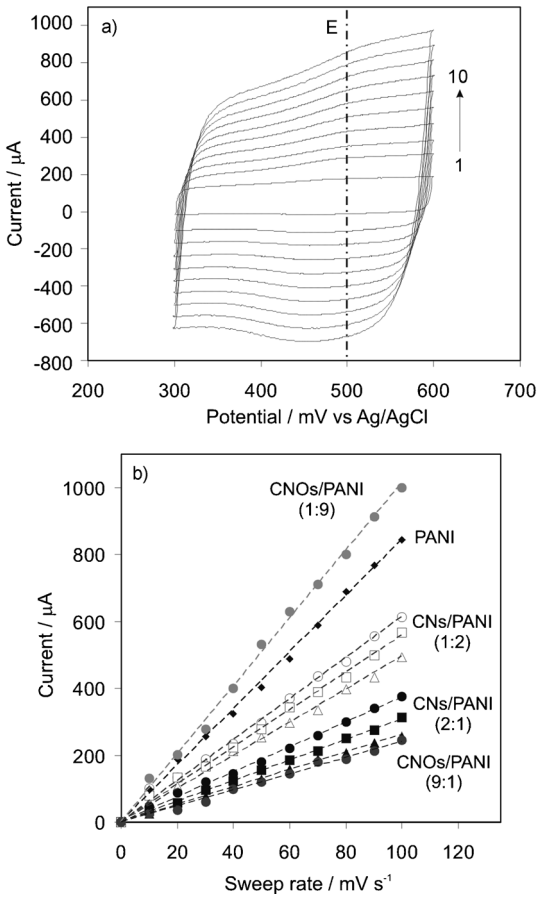

Figure 6. a) Cyclic voltammograms of the GC electrode covered with CNO/PANI (m_{CNOs}/m_{PANI} = 1:2) in 0.1 M H_2SO_4. The sweep rate was 1) 10, 2) 20, 3) 30, 4) 40, 5) 50, 6) 60, 7) 70, 8) 80, 9) 90, and 10) 100 mV s^{-1}. b) Dependence of the capacitive current with the sweep rate for CN/PANI at +500 mV in 0.1 M H_2SO_4. Mass ratio CN/PANI was: (●) 2:1 (CNO/PANI), (○) 1:2 (CNO/PANI), (◉) 1:9 (CNO/PANI), (■) 2:1 (MWNT/PANI), (□) 1:2 (MWNT/PANI), (▲) 2:1 (SWNT/PANI), (△) 1:2 (SWNT/PANI).

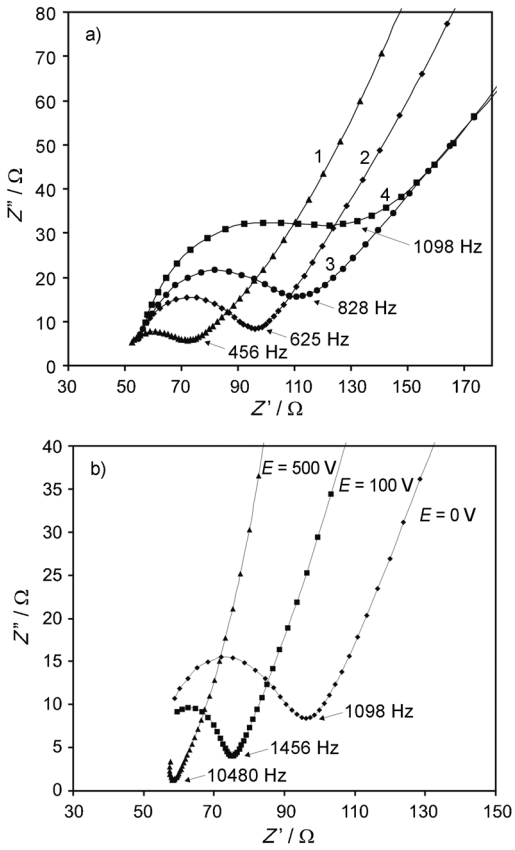

Figure 7. Complex-plane impedance plots for the GC electrode (1.6 mm) in 0.1 M H_2SO_4 covered with a) CNO/PANI (m_{CNOs}/mP_{ANI} = 9:1, 2:1, 1:2, 1:9) at 0 mV and b) CNO/PANI (m_{CNOs}/m_{PANI} = 1:2) at different potentials. Frequency was in the range of 100 kHz to 0.1 Hz.

that CNOs inside the PANI matrix result in faster electron transport in the bulk film and faster charge transfer at the composite film/solution interface relative to those at the PANI film/solution interface. This suggests that CNOs in composites provide more active sites for faradaic reactions and lead to a larger specific capacitance than for pure PANI. Thus, formation of charge-transfer complexes between the CNs and PANI results in enhanced electrical conductivity and lower resistance and facilitates charge transfer within the composites.

Figure 8 shows the Nyquist plots of the CN/PANI (CNs: CNO, MWNT, or SWNT) composites with different film compositions for each composite at a potential E = 500 mV versus Ag/AgCl. At this potential value, the impedance spectra display the expected shape for the double-layer charging of the porous electrodes,[57] without the semicircle resulting from electron-transfer-limited processes and an R_{CT} value of approximately 0. The Z' versus Z'' spectrum exhibits diffusion-controlled behavior at higher frequencies, which represents diffusion processes of the counterions within the polymer matrix and capacitive behavior at low frequencies.

The equivalent circuit for these composites was composed of the following elements (Figure 8): a bulk solution resistance (R_S); a constant phase element (CPE) connected in parallel to the resistance of the electrode/composite interface (R_{ct}); the Warburg impedance (Z_W), which represents the transport of counterions through the film during charging; and the elemental double-layer capacitance at a particular depth of the pore (C_p).[3] In addition, as a result of the porous structure of the electrode, a CPE element was used to express the double-layer capacitance (C_{dl}) at the carbon substrate and the contribution of the pseudocapacitance (C_F) of PANI, which is attributed to the faradaic process of PANI redox transition.[33]

The solid lines in Figure 8 are the impedance data representing the best-fit curves based on the equivalent circuit in Figure 9. The good fits reveal that this model successfully accounts for the electrochemical processes occurring on/within the CN/PANI composite electrodes. The best-fitting values from the EIS data for the electrochemical parameters corresponding to the circuit element are collected in Table 2. The impedance of the system is expressed by Equation (3):

$$Z(\omega) = R_S + Z_I(\omega) \quad (3)$$

The second part of the right side of this equation, that is, $Z_I(\omega)$, represents the process of composite charging and can be ex-

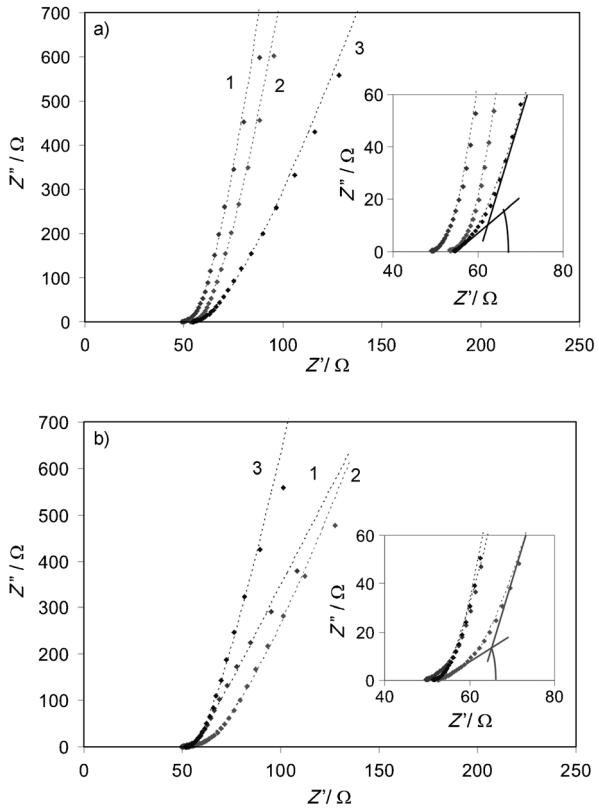

Figure 8. Complex-plane impedance plots for the GC electrode (1.6 mm) covered with CN/PANI a) $m_{CNs}/m_{PANI}=1:2$ or b) $m_{CNs}/m_{PANI}=2:1$ and 1) CNO/PANI, 2) MWNT/PANI, and 3) SWNT/PANI in 0.1 M H_2SO_4 at 500 mV. Frequency was in the range of 100 kHz to 0.1 Hz. Solid curves represent simulated data.

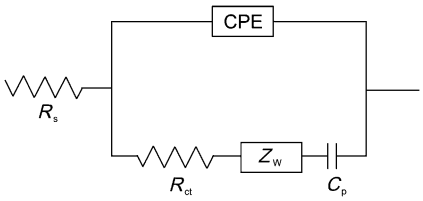

Figure 9. Equivalent electrical circuit representing the behavior of the CNs/PANI film electrodes in an electrolyte solution.

pressed by Equation (4):

$$\frac{1}{Z_I(\omega)} = \frac{1}{R_{ct}+Z_W} + j\omega C_{dl} \quad (4)$$

CPE can be defined as $1/Y_o(j\omega)^n$, in which Y_o is a constant with a dimension of *F*. It is associated with the roughness of the electrode surface and causes the rotation of the impedance to be at an angle of $(1-\alpha)90^\circ$. The Y_o value increases as the amount of the conducting polymer in the composite films increases (Table 2). In this study, some CN/PANI composites exhibit response composed of two lines with different slopes: a 45° line and a nearly vertical line (insets, Figure 8). The inclined line at low frequency is usually attributed to the porous structure of the electrode[59] or to the penetration of the electroactive species into the film.[60] Given that there is a little difference in the thickness of the deposited PANI films on the CNs, the inclined line could be attributed to the diffusion of ions in the active materials.[33] The vertical line at lower frequencies parallel to the *Z*" axis indicates capacitive behavior and represents the accumulation of diffused ions in the composite. As previously postulated, the absence of the 45° line suggests that the electrochemical reaction is limited to the surface layer of PANI in the CN/PANI films.[33]

Therefore, as seen from Table 2, the values of Y_o and *n* are strongly correlated. However, the *n* parameter obtained for all composites is very close to unity, which is indicative of almost-ideal capacitive behavior for these systems. Increasing the amount of PANI in the composites caused a decrease in *n*. A significant influence of the CN amount on the R_{ct} resistance is also observed. The value of R_{ct} decreases when the amount of CNs in the composite increases. This effect is probably related to differences in porosity and thickness of PANI in the composites. Specific capacitances (C_S) calculated from the Y_o and C_p parameters, C_{dl}, are close to the values obtained from CV (see Tables 1 and 2).

From the EIS measurements, the capacitance dependence with the frequency can be measured. The capacitance $C(\omega)$ can also be expressed in its complex form as Equation (5):

$$C(\omega) = C'(\omega) - jC''(\omega) \quad (5)$$

Table 2. Electrochemical impedance parameters determined by using 1.6 mm GC electrode coated with the CN/PANI composites in 0.1 M H_2SO_4.

Composite	R_S [Ω]	Y_0 [mF]	*n*	R_{ct} [Ω]	Z_W [Ω]	C_P [mF]	C_{dl} [mF]	C_S [F g^{-1}][b]	*t* [ms]	C_S [F g^{-1}][c]
CNOs/PANI[a]										
9:1	52.6	0.138	1.000	1.60	81	1.25	1.39	139	85	125
2:1	49.4	0.681	0.961	3.20	52	1.69	2.37	237	103	210
1:2	50.0	1.210	0.815	4.41	54	1.78	2.99	299	159	291
1:9	47.1	1.565	0.770	5.25	31	3.68	5.25	525	283	512
MWNT/PANI[a]										
2:1	53.5	0.310	0.906	1.89	53	1.39	1.70	170	90	165
1:2	53.1	0.799	0.836	5.63	81	2.26	3.06	306	252	295
SWNT/PANI[a]										
2:1	54.5	0.315	0.841	1.40	129	0.82	1.13	113	53	110
1:2	51.8	0.824	0.910	3.10	52	1.74	2.56	256	119	255
PANI	49.5	1.908	0.809	4.69	15	2.73	4.64	464	277	452

[a] The m_{CNs}/m_{PANI} mass ratio in the composite. [b] Capacitance per gram of the composite (from model). [c] Capacitance per gram of the composite calculated from the limiting value of the *C'* versus log *f* relation.

and the real [$C'(\omega)$] and imaginary [$C''(\omega)$] parts of the capacitance can be expressed by Equations (6) and (7):

$$C'(\omega) = \frac{-Z''(\omega)}{\omega|Z(\omega)|^2} \quad (6)$$

$$C''(\omega) = \frac{Z'(\omega)}{\omega|Z(\omega)|^2} \quad (7)$$

C' is calculated according to the complex capacitance model,[61] which suggests that the supercapacitor behaves like a series combination of a resistance and a capacitance according to Equation (7). The C'' versus log f dependences exhibit a maximum at a relaxation frequency (f_R). The relaxation frequency is related to the time constant (τ_R) of every electrode and can be calculated from Equation (8):

$$\tau_R = (2\pi f_R)^{-1} \quad (8)$$

The low τ_R value of 53 ms is preferred for electrochemical capacitors for fast charge–discharge processes.[62] Very good agreement between the values of specific capacitance (C_s) calculated from the model or from the limiting value of the C' versus log f relation, obtained from the faradaic impedance measurements and from voltammetric studies, was observed. The combination of CNs with PANI effectively increased the conductivity of the active layer.

3. Conclusion

CN/PANI (CN: CNO, MWNT, or SWNT) composite materials were synthesized by in situ chemical oxidative polymerization of aniline containing well-dispersed CNs. Composite films on glassy carbon electrode surfaces were deposited by a coating method by applying a drop of solution containing the suspended CN/PANI derivatives. The composites form relatively porous structures on the electrode surface and exhibit typical capacitive behavior, as well as excellent mechanical and electrochemical stability over a wide potential window (from $+0.30$ to $+0.60$ V vs. Ag/AgCl). The capacitance of the films is primarily controlled by the type of CN and their relative amounts in the composites. The highest specific capacitance of 525 F g^{-1} was obtained for the CNO/PANI ($m_{CNOs}/m_{PANI} = 1{:}9$) composite films. CNs improve the properties of the composite films, and this makes them more active for faradaic reactions, which confers larger specific capacitances, lower resistances, and better cyclic stability than for pure PANI. The CNO/PANI composites described here can be effectively used as electrodes for supercapacitors.

Experimental Section

Materials

Synthesis of CNs/PANI: The CNs (30 mg), 4-aminobenzoic acid (4-ABAc, 30 mg), and polyphosphoric acid (pPAc, 1200 mg) were placed in a flask equipped with a high torque mechanical stirrer, nitrogen inlet, and outlet. This mixture was stirred under a dry nitrogen atmosphere. The reaction mixture was heated to 80 °C for 1 h, to 100 °C for another 1 h, and finally to 130 °C for 72 h.[63] The mixture was poured into deionized water, left for 3 d, and then poured into methanol and left for another 3 d. The CN/4-ABAc derivatives were dried overnight in an oltam oven ($T = 60$ °C). The modified CNs (15 mg) were dispersed by ultrasonication for 30 min in 1 M HCl (25 mL). The polymerization of aniline was performed by following a published procedure.[64] Four different concentrations of aniline monomers (i.e. 15.76, 47.27, 94.54, and 141.81 mg) were dispersed into 1 M HCl (15 mL), and the mixture was stirred for 30 min in an ice bath. The CN/4-ABAc derivative was cooled down and added to aniline, and the mixture was stirred for another 30 min. Ammonium peroxydisulfate (50 mg) was dissolved in 1 M HCl (5 mL) and added very slowly to the mixture. The polymerization was carried out at 0–5 °C over 4 h. Products were washed several times with 0.2 M HCl and acetone and dried overnight in an oven ($T = 50$ °C). The content of CN in the CN/PANI samples was 88, 65, 32, and 11% CNO (9:1, 2:1, 1:2, and 1:9 mass ratio CNO/PANI); 69 and 31% (2:1 and 1:2 mass ratio SWNT/PANI); and 64 and 33% MWNT (2:1 and 1:2 mass ratio MWNT/PANI).

Preparation of CN/PANI films: The CN/PANI (CN: CNO, SWNT, or MWNT) composite (2 mg) was dispersed with the aid of ultrasonic agitation in dichloromethane (1 mL) to give a black suspension (2 mg mL^{-1}). The CN/PANI (CN: CNO, SWNT, or MWNT) films were prepared by the cast method. A solution of CN/PANI (2 mg mL^{-1}, 10 μL) was transferred to the GC (1.5 mm diameter) surface, and the solvent was evaporated under an argon atmosphere.

Methods

Spectra of the PANI-coated CNs were recorded with a Nicolet iN10 MX FTIR microscope (Thermo Scientific) equipped with a mercury cadmium telluride (MCT) liquid nitrogen cooled detector. Samples were placed on the gold plate without any further preparation. Spectra were recorded in the reflectance mode.

The films were imaged by secondary electron SEM with an INSPECT S50 scanning electron microscope from FEI. The accelerating voltage of the electron beam was 20 keV, and the working distance was 10 mm. TEM images were recorded with a FEI Tecnai transmission electron microscope. The accelerating voltage of the electron beam was 200 keV.

Voltammetric experiments were performed with an AUTOLAB (Utrecht, The Netherlands) computerized electrochemistry system equipped with the PGSTAT 12 potentiostat and FRA response analyzer expansion cards with a three-electrode cell. The AUTOLAB system was controlled with the GPES 4.9 software of the same manufacturer. A glassy carbon disk electrode (Bioanalytical Systems, Inc.) with a diameter of 1.6 mm (Bioanalytical Systems, Inc.) was used as the working electrode. The surface of the electrode was polished by using extra-fine carborundum paper (Buehler) followed by 0.3 μm alumina and 0.25 μm diamond polishing compound (Metadi II, Buehler). The electrode was then sonicated in water to remove trace amounts of alumina from the metal surface, washed with water, and dried. The counterelectrode was a platinum flag with an area of about 0.5 cm^2. A silver wire immersed in 0.1 M AgCl and separated from the working electrode by a ceramic tip (Bioanalytical Systems, Inc.) served as the reference electrode. All experiments were done in water purified through a Millipore apparatus. Oxygen was removed from the solution by purging with argon.

Acknowledgements

The authors thank Adrián Villalta-Cerdas (Clemson University, USA) for CNO synthesis. We gratefully acknowledge the financial support of the NCN, Poland (grant no. 2011/01/B/ST5/06051 to M.E.P.-B. and NN204396640). L.E. thanks the Robert A. Welch Foundation for an endowed chair (grant no. AH-0033), and the US NSF (grant CHE-1110967). TEM, SEM, and potentiostat were funded by the European Fund for Regional Development and National Fund—Ministry of Science and Higher Education as part of the Operational Programme Development of Eastern Poland 2007–2013 (project: POPW.01.03.00-20-034/09-00).

Keywords: charge transfer · electrochemistry · nanostructures · conducting materials · polymers

[1] F. Beguin, E. Frackowiak, *Nanotextured Carbons for Electrochemical Energy Storage, Handbook of Nanomaterials No. 26* (Ed.: Y. Gogotsi), CRC, Boca Raton, **2006**.
[2] C.-W. Huang, Y.-T. Wu, Ch.-Ch. Hu, Y.-Y. Li, *J. Power Sources* **2007**, *172*, 460 – 467.
[3] R. Kötz, M. Carlen, *Electrochim. Acta* **2000**, *45*, 2483 – 2498.
[4] J. P. Zheng, T. R. Jow, *J. Electrochem. Soc.* **1995**, *142*, L6 – L7.
[5] C. C. Hu, W. C. Chen, *Electrochim. Acta* **2004**, *49*, 3469 – 3477.
[6] J. W. Long, K. E. Ayers, D. R. Rolison, *J. Electroanal. Chem.* **2002**, *522*, 58 – 65.
[7] F. Fusalba, P. Gouerec, D. Villers, D. Belanger, *J. Electrochem. Soc.* **2001**, *148*, A1 – A6.
[8] C.-C. Hu, X.-X. Lin, *J. Electrochem. Soc.* **2002**, *149*, A1049 – A1057.
[9] J. P. Ferraris, M. M. Eissa, J. D. Brotherson, D. C. Loveday, A. A. Moxey, *J. Electroanal. Chem.* **1998**, *459*, 57 – 69.
[10] E. Frackowiak, U. Beguin, *Carbon* **2001**, *39*, 937 – 950.
[11] D. Qu, H. Shi, *J. Power Sources* **1998**, *74*, 99 – 107.
[12] J. Gamby, P. L. Taberna, P. Simon, J. F. Fauvarque, M. Chesneau, *J. Power Sources* **2001**, *101*, 109 – 116.
[13] D. E. Stilwell, S.-M. Park, *J. Electrochem. Soc.* **1988**, *135*, 2254 – 2262.
[14] J. P. Zheng, P. G. Cygan, T. R. Jow, *J. Electrochem. Soc.* **1995**, *142*, 2699 – 2703.
[15] J. J. Park, O. O. Park, K. H. Shin, C. S. Jin, J. H. Kim, *Electrochem. Solid-State Lett.* **2002**, *5*, H7 – H10.
[16] E. Frackowiak, V. Khomenko, K. Jurewicz, K. Lota, F. Beguin, *J. Power Sources* **2006**, *153*, 413 – 418.
[17] B. Dong, B.-L. He, C.-L. Xu, H.-L. Li, *Mater. Sci. Eng. B* **2007**, *143*, 7 – 13.
[18] W. Xing, S. Zhou, H. Cui, W. Si, X. Gao, Z. Yan, *J. Porous Mater.* **2008**, *15*, 647 – 651.
[19] E. Frackowiak, K. Jurewicz, S. Delpeux, F. Beguin, *J. Power Sources* **2001**, *97-98*, 822 – 825.
[20] J. Zhu, H. Gu, Z. Luo, N. Haldolaarachige, D. P. Young, S. Wei, Z. Guo, *Langmuir* **2012**, *28*, 10246 – 10255.
[21] L. Agüí, C. Peña-Farfal, P. Yáñez-Sedeño, M. J. Pingarrón, *Electrochim. Acta* **2007**, *52*, 7946 – 7952.
[22] C. A. Furtado, U. J. Kim, H. R. Gutierezz, L. Pan, E. C. Dickey, P. C. Eklund, *J. Am. Chem. Soc.* **2004**, *126*, 6095 – 6105.
[23] Z. Mandić, M. K. Roković, T. Pokupčić, *Electrochim. Acta* **2009**, *54*, 2941 – 2950.
[24] J. Stejskal, I. Sapurina, M. Trchova, E. N. Konyusenko, P. Holler, *Polymer* **2006**, *47*, 8253 – 8262.
[25] M. Mazur, M. Tagowska, B. Palys, K. Jackowska, *Electrochem. Commun.* **2003**, *5*, 403 – 407.
[26] J. Desilvestro, W. Scheifele, *J. Mater. Chem.* **1993**, *3*, 263 – 272.
[27] M. Grzeszczuk, G. Zabinska-Olszak, *J. Electroanal. Chem.* **1993**, *359*, 161 – 174.
[28] L. Duić, M. Kralijć, S. Grigić, *J. Polym. Sci. Part A* **2004**, *42*, 1599 – 1608.
[29] C. Xiang, Q. Xie, J. Hu, S. Yao, *Synth. Met.* **2006**, *156*, 444 – 447.
[30] M. Cochet, W. K. Maser, A. M. Benito, M. A. Callejas, M. T. Martinez, J. M. Benoit, J. Schreiber, O. Chauvet, *Chem. Commun.* **2001**, 1450 – 1451.
[31] V. Gupta, N. Miura, *Electrochim. Acta* **2006**, *52*, 1721 – 1726.
[32] J. Zhang, I. B. Kong, B. Wang, Y. C. Luo, I. Kang, *Synth. Met.* **2009**, *159*, 260 – 266.
[33] S.-B. Yoon, E.-H. Yoon, K.-B. Kim, *J. Power Sources* **2011**, *196*, 10791 – 10797.
[34] Ch. Meng, Ch. Liu, S. Fan, *Electrochem. Commun.* **2009**, *11*, 186 – 189.
[35] L. X. Li, H. H. Song, Q. C. Zhang, J. Y. Yao, X. H. Chen, *J. Power Sources* **2009**, *187*, 268 – 274.
[36] J. Yan, T. Wei, Z. Fan, W. Qian, M. Hang, X. Shen, F. Wei, *J. Power Sources* **2010**, *195*, 3041 – 3045.
[37] D. Ugarte, *Nature* **1992**, *359*, 707 – 709.
[38] S. Iijima, *J. Cryst. Growth* **1980**, *50*, 675 – 683.
[39] S. Iijima, *J. Phys. Chem.* **1987**, *91*, 3466 – 3467.
[40] R. Bacon, *J. Appl. Phys.* **1960**, *31*, 283 – 290.
[41] V. L. Kuznetsov, A. L. Chuvilin, Y. V. Butenko, I. Y. Malkov, V. M. Titov, *Chem. Phys. Lett.* **1994**, *222*, 343 – 351.
[42] E. Koudoumas, O. Kokkinaki, M. Konstantaki, S. Couris, S. Korovins, P. Detkov, V. Kuznetsov, S. Pimenov, V. Pustovoi, *Chem. Phys. Lett.* **2002**, *357*, 336 – 340.
[43] M. Choi, I. S. Altman, Y. J. Kim, P. V. Pikhitsa, S. Lee, G. S. Park, T. Jeong, J. B. Yoo, *Adv. Mater.* **2004**, *16*, 1721 – 1725.
[44] H. Wang, T. Abe, S. Maruyama, Y. Iriyama, Z. Ogumi, Z. Yoshikawa, *Adv. Mater.* **2005**, *17*, 2857 – 2860.
[45] Y. Liu, R. L. Vander Wal, V. N. Khabashesku, *Chem. Mater.* **2007**, *19*, 778 – 786.
[46] J. Luszczyn, M. E. Plonska-Brzezinska, A. Palkar, A. T. Dubis, A. Simionescu, D. T. Simionescu, B. Kalska-Szostko, K. Winkler, L. Echegoyen, *Chem. Eur. J.* **2010**, *16*, 4870 – 4880.
[47] M. E. Plonska-Brzezinska, A. Palkar, K. Winkler, L. Echegoyen, *Electrochem. Solid-State Lett.* **2010**, *13*, K35 – K38.
[48] J. Breczko, K. Winkler, M. E. Plonska-Brzezinska, A. Villalta-Cerdas, L. Echegoyen, *J. Mater. Chem.* **2010**, *20*, 7761 – 7768.
[49] M. E. Plonska-Brzezinska, J. Mazurczyk, J. Breczko, B. Palys, A. Lapinski, L. Echegoyen, *Chem. Eur. J.* **2012**, *18*, 2600 – 2608.
[50] M. N. Vijayashree, S. V. Subramanyam, A. G. Samuelson, *Macromolecules* **1992**, *25*, 2988 – 2990.
[51] Y. Furukawa, F. Ueda, Y. Ohydo, I. Harada, T. Nakajima, T. Kawagoe, *Macromolecules* **1988**, *21*, 1297 – 1305.
[52] S. Quillard, G. Louarn, S. Lefrant, A. G. MacDiarmid, *Phys. Rev. B* **1994**, *50*, 12496 – 12508.
[53] G. E. Asturias, A. G. MacDiarmid, R. P. McCall, A. J. Epstein, *Synth. Met.* **1989**, *29*, 157 – 162.
[54] Z. Ping, G. E. Nauer, H. Neugebauer, J. Theiner, A. Neckel, *Electrochim. Acta* **1997**, *42*, 1693 – 1700.
[55] A. K. Mishra, P. Tandon, V. D. Gupta, *Macromol. Symp.* **2008**, *265*, 111 – 123.
[56] D. E. Stilwell, S. M. Park, *J. Electrochem. Soc.* **1988**, *135*, 2491 – 2497.
[57] Y. Wei, W. W. Focke, G. E. Wnek, A. Ray, A. G. MacDiarmid, *J. Phys. Chem.* **1989**, *93*, 495 – 499.
[58] E. Barsoukov, J. R. MacDonald, *Impedance Spectroscopy Theory, Experiment, and Applications, 2nd ed.*, Wiley, Hoboken, **2005**.
[59] S. Zhang, C. Peng, K. C. Ng, G. Z. Chen, *Electrochim. Acta* **2010**, *55*, 7447 – 7453.
[60] A. J. Roberts, R. C. T. Slade, *Electrochim. Acta* **2010**, *55*, 7460 – 7469.
[61] P. I. Taberna, P. Simon, J. F. Fauvarque, *J. Electrochem. Soc.* **2003**, *150*, A292 – A300.
[62] S. Burke, *J. Power Sources* **2000**, *91*, 37 – 50.
[63] H. J. Lee, S. W. Huo, Y. D. Kwon, L. S. Tan, J. B. Baek, *Carbon* **2008**, *46*, 1850 – 1859.
[64] J. Stejskal, R. G. Gilbert, *Pure Appl. Chem.* **2002**, *74*, 857 – 867.

Received: September 15, 2012
Published online on November 30, 2012